ResearchGate

See discussions, stats, and author profiles for this publication at: http://www.researchgate.net/publication/3101799

Nondiagonally anisotropic PML: A generalized unsplit wide-angle absorber for the treatment of the near-grazing effect in FDTD meshes

ARTICLE *in* IEEE TRANSACTIONS ON MAGNETICS · AUGUST 2000

Impact Factor: 1.21 · DOI: 10.1109/20.877590 · Source: IEEE Xplore

CITATIONS
3

DOWNLOADS
30

VIEWS
64

4 AUTHORS, INCLUDING:

Theodoros Kosmanis
Alexander Technological Educational Institut…

26 PUBLICATIONS **82** CITATIONS

SEE PROFILE

Available from: Theodoros Kosmanis
Retrieved on: 02 July 2015

Nondiagonally Anisotropic PML: A Generalized Unsplit Wide-Angle Absorber for the Treatment of the Near-Grazing Effect in FDTD Meshes

Nikolaos V. Kantartzis, *Student Member, IEEE*, Traianos V. Yioultsis, Theodoros I. Kosmanis, *Student Member, IEEE*, and Theodoros D. Tsiboukis, *Senior Member, IEEE*

***Abstract*—A new generalization of the PML with wide-angle absorption is presented, for the efficient truncation of FDTD lattices. The proposed unsplit-field layer uses a nondiagonal symmetric tensor anisotropy and via an appropriate parameter selection achieves notable attenuation rates in the case of near-grazing angles. Hence, it can be placed much closer to large structures. Improved accuracy and lower dispersion errors are attained via higher-order FDTD schemes with regular and non-Cartesian lattices constructed by hexagonal or tetradecahedral cells. Finally, Ramahi ABC's are invoked for the absorber's termination. Numerical results, addressing wave attenuation at grazing incidence, prove the efficiency of the proposed PML.**

***Index Terms*—Electromagnetic scattering, FDTD methods, numerical analysis, perfectly matched layers.**

I. Introduction

THE ADVENT of the Perfectly Matched Layer (PML) [1] for the treatment of electromagnetic scattering and radiation problems, had a decisive impact on the quality and performance of numerical algorithms and specifically the FDTD method [2], [3]. However, several shortcomings have been detected, like the inadequate absorption of evanescent waves, the dispersion and anisotropy errors, as well as the near-grazing incidence effect. Over the recent years, various techniques have been introduced. The physical interpretation of the PML using complex coordinate stretching is given in [4], [5]. Moreover, other schemes based on uniaxial tensor PML mapping in rectangular cells, have been presented for the FEM [6], [7] and the FDTD method [8]–[12], while [13] introduces an interesting noncubic absorbing layer. Finally, a higher-order reflectionless sponge layer is discussed in [14].

Lately, a generalized nondiagonal PML with wide-angle absorption has been introduced and applied in FEM scattering analysis [15]. The fundamental attributes of this novel absorber are the fully nondiagonal symmetric complex tensors and its ability to model waves with grazing incidence. In this paper, we propose a new completely Maxwellian formulation of this anisotropic PML for the 3-D FDTD method, to avoid the nonphysical field splitting. Theoretical analysis reveals that an appropriate choice of its parameters yields significant absorption in the case of grazing incidence, where existing approaches lack to provide acceptable annihilation. The dispersion errors are suppressed via efficient higher-order FDTD (conventional or nonstandard) schemes in regular and non-Cartesian grids with hexagons [13] and tetradecahedra. Temporal integration is alternatively performed by the Runge–Kutta integrator, while Complementary Operators (COM) [16] are used for the termination of the absorber. Finally, the proposed PML is validated through diverse simulations.

Manuscript received October 25, 1999.

The authors are with the Department of Electrical and Computer Engineering, Aristotle University of Thessaloniki, GR 54006, Greece (e-mail: tsibukis@eng.auth.gr).

Publisher Item Identifier S 0018-9464(00)05360-7.

II. Theory of the Nondiagonally Anisotropic PMLs

The novel PML is composed of an artificial anisotropic material, characterized by fully nondiagonal symmetric complex constitutive tensors, written in the form of

$$\bar{\bar{\varepsilon}}_r = \bar{\bar{\mu}}_r = \bar{\bar{\Lambda}} = \begin{bmatrix} a & g & u \\ g & b & h \\ u & h & c \end{bmatrix} \tag{1}$$

The parameters in (1) must be defined, so that the medium is reflectionless for plane waves of any incidence angle. In the uniaxial PML, parameters are obtained by requiring that the reflection coefficient is zero for every angle of incidence [6]. In the case of nondiagonal tensor, the explicit derivation of this coefficient is a complicated task, though. We overcome this by enforcing the *a priori* reflectionless character of the layer, which along with the boundary conditions and the dispersion relation, results in the unknown PML parameters.

We begin with Maxwell's curl equations, which, due to the nondiagonal tensor, are strongly coupled. Their solution in terms of the wave number, is very difficult, and leads to odd and even modes to be considered. Hence, we assume no reflection from the interface (Fig. 1) and then apply the proper tangential/normal continuity conditions. For a TE wave, the incident and transmitted electric fields are

$$\boldsymbol{E}_i = E_0 e^{-jk_s(\sin\theta_i x + \cos\theta_i z)}\hat{\boldsymbol{y}} \quad \text{with} \quad k_s = \omega\sqrt{\mu\varepsilon}, \tag{2}$$

$$\boldsymbol{E}_t = E_0(\hat{\boldsymbol{y}} - hc^{-1}\hat{\boldsymbol{z}})e^{-j(k_x x + k_y y + k_z z)}, \tag{3}$$

in which the reflected field is by definition zero and the nondiagonal tensor introduces a z-component in (3). If $\boldsymbol{E}$ tangential components are phase matched, we obtain

$$k_x = k_s \sin\theta_i, \qquad k_y = 0. \tag{4}$$

0018–9464/00$10.00 © 2000 IEEE

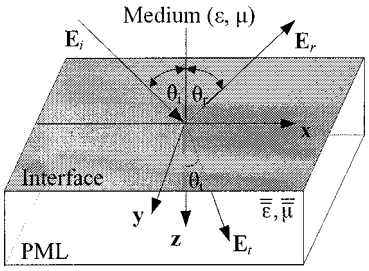

Fig. 1. Plane wave incidence on the medium-PML interface.

Substitution of (2) and (3) to Maxwell's equations provides the magnetic incident and transmitted waves

$$\boldsymbol{H}_i = \eta^{-1} E_0 (-\cos\theta_i \hat{\boldsymbol{x}} + \sin\theta_i \hat{\boldsymbol{z}}) e^{-jk_s(\sin\theta_i x + \cos\theta_i z)}, \quad (5)$$

$$\begin{aligned}\boldsymbol{H}_t = {} & (k_s\eta)^{-1} E_0 \\ & \cdot \left\{ \left[-a' k_z + \left(\frac{hg'}{c} + u' \right) k_x \right] \hat{\boldsymbol{x}} \right. \\ & - \left[g' k_z + \left(\frac{hb'}{c} + h' \right) k_x \right] \hat{\boldsymbol{y}} \\ & \left. + \left[-u' k_z + \left(\frac{hh'}{c} + c' \right) k_x \right] \hat{\boldsymbol{z}} e^{-j(k_x x + k_z z)} \right\}, \end{aligned} \quad (6)$$

where the primed symbols are the elements of tensor $\overline{\overline{\Lambda}}^{-1}$, arranged in a way similar to (1). Likewise, boundary conditions are enforced to the magnetic field intensity $\boldsymbol{H}$ (tangential continuity) and flux density $\boldsymbol{B}$ (normal continuity). Amplitude and phase matching, give

$$uh = gc, \qquad k_z = k_s(\cos\theta_i + u' \sin\theta_i)/a'. \quad (7)$$

The dispersion relation can now be found by decomposing (5) along with the aforementioned boundary conditions. Since a diagonal decomposition is not feasible due to algebraic complexity, the whole procedure can be further simplified if we exploit the *a priori* expressions (2), (3). Consequently,

$$ak_x^2 + ck_z^2 + 2uk_x k_z = k_s^2 c^{-1}(ac - u^2)(bc - h^2). \quad (8)$$

Enforcing (7) to (8) the set of constraints among the PML parameters is fully completed with the relations

$$ac - u^2 = 1, \qquad bc - h^2 = 1. \quad (9)$$

The final form of tensor (1), which renders the medium reflectionless, is derived by combining (8) with (7) and (9),

$$\overline{\overline{\Lambda}} = \begin{bmatrix} (1+u^2)c^{-1} & u^2 c^{-1} & u \\ u^2 c^{-1} & (1+u^2)c^{-1} & u \\ u & u & c \end{bmatrix}. \quad (10)$$

For clarity, we have set $h = u$ in order to have the same layer properties toward directions on the transversal plane. As it can be observed, (10) involves two complex parameters (four real degrees of freedom) which can be properly selected, without loss of generality, to be of the following form

$$c^{-1} = q - j\sigma \quad \text{with} \quad q, \sigma \geq 0, \quad (11)$$

where σ can be considered the layer's conductivity and q a parameter controlling the angle of propagation. Transmission inside PML is proven to be described by

$$\boldsymbol{E}_t = \boldsymbol{E}_0^t e^{-k_s \sigma z(\cos\theta_i - u\sin\theta_i)} e^{-jk_s q z(\cos\theta_i - u\sin\theta_i)}, \quad (12)$$

with an angle of $\theta_t = \tan^{-1}\{\sin\theta_i / [q(\cos\theta_i - u\sin\theta_i)]\}$.

Parameter u plays an important role in the PML annihilation mechanism. If $u < 0$, the damping factor in (12) is further enhanced. Contrary to standard PML's, where the cosine term is negligible for near-grazing incidence, the proposed scheme achieves considerable attenuation, since the new sine term is maximized. Moreover, the PML behavior is improved at all intermediate angles. Wide-angle absorption is very advantageous in the analysis of large structures as it enables the placement of PML closer to the scatterer, with an obvious reduction of the computational burden.

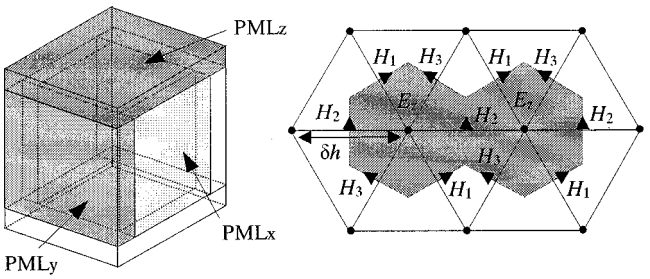

Fig. 2. (a) Structure of the PML regions. (b) Hexagonal staggered lattice.

III. FDTD Implementation of the New PMLs

Let us consider a linear, isotropic medium, surrounded by nondiagonal PML's, constructed in two different ways. First, with the scheme of [8] and second with the one shown in Fig. 2(a). Its merit is the absence of overlapping PML areas such as edge or corners (requiring special treatment), thus simpler FDTD analysis. From numerical simulations, both techniques were found equivalently efficient. Since the former is known, we will focus on the study of the latter.

A. Construction Procedure and Time-Domain Simulations

The PML layers in Fig. 2(a), are structurally similar. Their difference is the cyclic permutation of the elements in (10). Consider layer PMLz. Due to the nondiagonal form of the tensor, Maxwell's equations for the $\boldsymbol{E}$ (or $\boldsymbol{H}$) components result in a 3×3 linear system, the solution of which gives

$$j\omega\varepsilon c^{-1} E_{x,y} = (\nabla \times \boldsymbol{H})_{x,y} - \frac{1}{c} u (\nabla \times \boldsymbol{H})_z, \quad (13)$$

$$\begin{aligned} j\omega\varepsilon E_z = {} & \frac{1}{c}(1+2u^2)(\nabla \times \boldsymbol{H})_z \\ & - u[(\nabla \times \boldsymbol{H})_x + (\nabla \times \boldsymbol{H})_y]. \end{aligned} \quad (14)$$

The FDTD analogues of (13), (14) are derived through the proper Fourier transform and $\sigma = \sigma'/\omega$. Hence,

$$q\partial_t E_{x,y} + \sigma' E_{x,y} = \frac{1}{\varepsilon}[\boldsymbol{F}_{x,y} - uI(t) - uq\boldsymbol{F}_z], \tag{15}$$

$$\partial_t E_z = \frac{1}{\varepsilon}\{(1+2u^2)[q\boldsymbol{F}_z + I(t)] - u[\boldsymbol{F}_x + \boldsymbol{F}_y]\}. \tag{16}$$

where $\boldsymbol{F} = \nabla \times \boldsymbol{H}$ and $I(t) = \sigma' \int_0^t (\nabla \times \boldsymbol{H})_z \, dt'$.

Notice that if $u = 0$, (15) and (16) reduce to the unsplit-field PML expressions. The time integral, $I(t)$, of the z-component of $\boldsymbol{F}$, can be viewed as a field-dependent source. Its numerical computation is performed via the trapezoidal rule

$$\int_0^{n\delta t} \boldsymbol{F}_z \, dt' = \sum_{m=0}^{n-1} \boldsymbol{F}_z^m \delta t + \tfrac{1}{2}\boldsymbol{F}_z^n \delta t, \tag{17}$$

in which superscripts m, n denote the time at which the respective quantity is calculated. For instance, (15) becomes

$$E_{x,y}^{n+1} = (q - \sigma'\delta t)E_{x,y}^n + \frac{\delta t}{\varepsilon}\begin{bmatrix} \boldsymbol{F}_x^{n+0.5} - u\left(\dfrac{\sigma'\delta t}{2} + q\right)\boldsymbol{F}_z^{n+0.5} \\ -u\sigma'\delta t W_z^{n-0.5} \end{bmatrix} \tag{18}$$

where W_z is defined and updated by

$$W_z^{n-0.5} = \sum_{m=0}^{n-0.5} \boldsymbol{F}_z^m \quad \text{with} \quad W_z^{n+0.5} = W_z^{n-0.5} + \boldsymbol{F}_z^{n+0.5}. \tag{19}$$

As an alternative, the auxiliary two-step equation technique was also utilized. According to this algorithm, the evaluation of the time integral is avoided, at the expense of an additional equation which updates the respective flux density component introduced for the substitution of the integral term.

B. Non-Cartesian Lattices and Higher-Order Schemes

The basic feature of the non-Cartesian grids is the approximation of spatial operators by data located not only along the axes, but also on other positions. Thus, derivatives are precisely calculated. We consider the 2-D hexagonal mesh based on 7-point stencils (tetradecahedral in 3-D), as in Fig. 2(b). The primary grid is discretized into hexagons, composed of equilateral triangles at the edge centers of which three normal $\boldsymbol{H}$ components are defined. The dual grid comprises canonical hexagons too and $\boldsymbol{E}$ components are placed at face centers. By relating the six nearest neighbors, we obtain the equation as shown in (20) at the bottom of the page.

To achieve superior accuracy, higher-order conventional and nonstandard FDTD schemes are combined with the above grids. Their advantages are the introduction of additional attenuation terms, toward different directions, in the PML, and the drastically limited number of points per wavelength (almost 1/250 that of Yee). The nonstandard derivatives are

$$\boldsymbol{LT}^{nst}[f] = \frac{1}{s_\omega(\delta t)}\left(f\big|_x^{t+\delta t/2} - f\big|_x^{t-\delta t/2}\right) - \frac{\delta t^2}{24}\partial_t^3 f\big|_x^t,$$

$$\boldsymbol{LS}_x^{nst}[f] = \tfrac{11}{12}\boldsymbol{L}_{x,\delta x}^{nst}[f] + \tfrac{1}{24} \cdot \left[\boldsymbol{L}_{x,3\delta x}^{nst}[f] + \frac{1}{\delta x}\left(f\big|_{x-(\delta x/2)}^t - f\big|_{x-(3\delta x/2)}^t\right)\right],$$

where the new 3-D operator $\boldsymbol{L}_{x,\delta h}^{nst}$ $(\delta h = \delta x, 3\delta x)$ is defined as

$$\boldsymbol{L}_{x,\delta h}^{nst}[f] \equiv \frac{1}{s_k(\delta h)}\left(\zeta_1 \boldsymbol{p}_{x,\delta h}^{(1)}[f] + \zeta_2 \boldsymbol{p}_{x,\delta h}^{(2)}[f] + \zeta_3 \boldsymbol{p}_{x,\delta h}^{(3)}[f]\right). \tag{21}$$

The $s_\omega(\delta t)$, $s_k(\delta h)$ are proper correction functions, ζ are parameters which render stability and well-posedness, while $\boldsymbol{p}$ are difference forms constructed for error minimization. The wider spatial stencils are treated by compact operators, whereas the fourth-order Runge–Kutta integrator is used as an alternative time integration scheme. It is mentioned that one of the motives for the choice of the higher-order (HO) FDTD schemes is the efficient treatment of the resulting odd and even modes. Finally, the accurate COM is imposed on the outer PML boundaries instead of the usual PEC walls.

IV. Numerical Results

The proposed PML's are verified via 2-D and 3-D FDTD simulations regarding scattering from different materials. Computations are performed in a finite domain A, embedded in the center of a much larger reference domain B terminated by the second-order Ramahi ABC's. Excitation is provided by a compact smooth pulsed electric source (TM case)

$$E_z = \frac{1}{320}\left(12 - 15\cos\frac{2\pi}{T}t + 6\cos\frac{4\pi}{T}t - 3\cos\frac{6\pi}{T}t\right), \tag{22}$$

supported in $t \in [0, T]$ with $T = 1$ nsec. Domain A is discretized by an initial cubic grid with a cell size of 0.012 m and a time step of 85% the Courant limit. It is stated that the HO and hexagonal FDTD concepts enable the use of coarser grids.

In Figs. 3 and 4 we show the global and local errors induced by uniaxial (D) and nondiagonal (ND) PML's for a domain $A = 2\lambda \times 2\lambda \times 2\lambda$ with a scatterer of electrical size 1.7 and relative permittivity 2.5. Domain B is large enough to allow for a causal isolation. The scatterer-PML distance is initially 0.15λ. As it can be observed, a proper choice of tensor parameters gives a notable reduction of reflection. Such global errors (10^{-10} or better) are highly desirable, since they correspond to an actual normalized local error of 10^{-4}–10^{-5}. Moreover, although the error is shown for 500 steps, we have not encountered any instabilities for larger simulation times. We also emphasize that

$$\frac{\partial E_{z(i,j)}}{\partial t} = \frac{2}{3\varepsilon_0 \delta h}\begin{bmatrix} H_{1(i+(1/4),\, j-(\sqrt{3}/4))} - H_{1(i-(1/4),\, j+(\sqrt{3}/4))} + H_{2(i+(1/2),\, j)} \\ -H_{2(i-(1/2),\, j)} + H_{3(i+(1/4),\, j+(\sqrt{3}/4))} - H_{3(i-(1/4),\, j-(\sqrt{3}/4))} \end{bmatrix}. \tag{20}$$

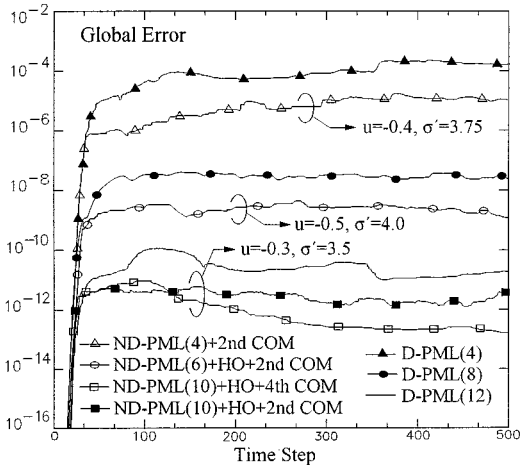

Fig. 3. Global error created by uniaxial (D) and nondiagonal (ND) PML's for different numbers of layers, higher-order (HO) schemes and COM backing.

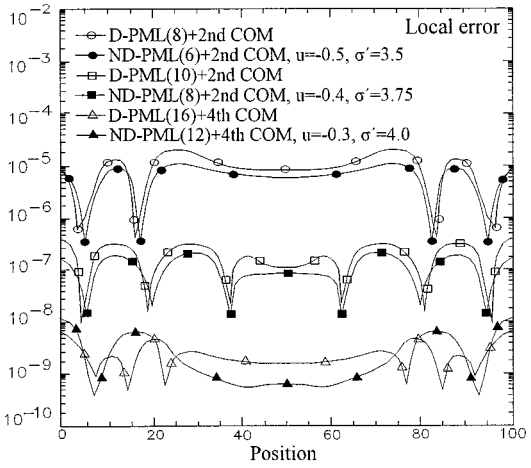

Fig. 4. Local error created by the uniaxial and nondiagonal PML schemes for different numbers of layers and PML parameters.

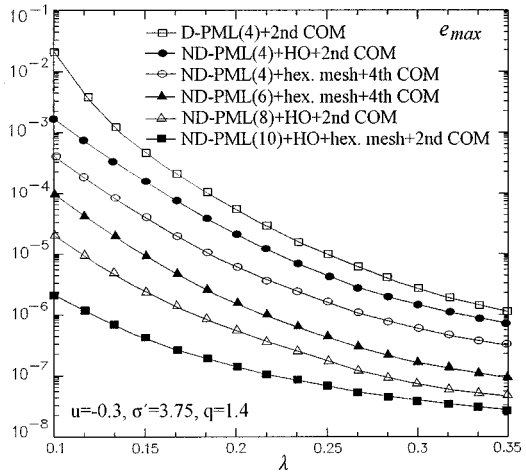

Fig. 5. The maximum global error vs. distance from the scatterer for various numbers of layers and diverse differencing (HO, hexagonal) schemes.

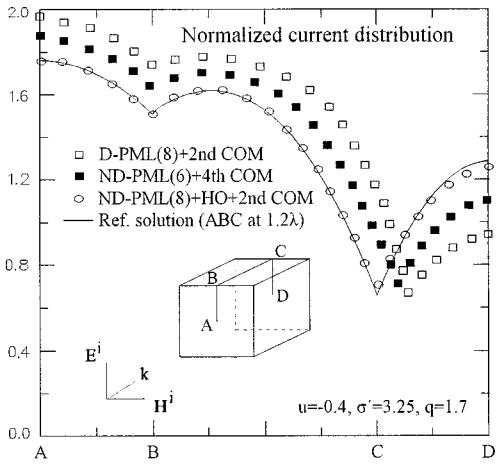

Fig. 6. Normalized surface current distribution along an E-plane loop.

one of the most prominent attributes of PML is its remarkable stability properties, as opposed to local ABC's, without any additional convergence requirement, except of that imposed by the Courant condition.

The behavior of the proposed PML's versus their distance from the scatterer, is studied in Fig. 5, where the maximum value of the global error is shown for every simulation. A 2-D domain $A = 2.2\lambda \times 2.2\lambda$ is considered and a PEC scatterer of electrical size 1.8 is incorporated. The combination of the HO nonstandard schemes together with the hexagonal meshes, are used for the PML realization. Results demonstrate a serious reduction of the error especially with the non-Cartesian lattices. We stress the improvement of maximum global error at 0.1λ, which implies remarkable savings in computational resources. As a result, the use of the ND-PML, especially with HO differencing schemes can decrease its distance from the scatterer at the very low level of 0.1λ, i.e. one cell only. However, a suggested distance would be $0.15 \div 0.2\lambda$, where the error is one or two orders of magnitude lower.

Scattering from a PEC cube of electrical size equal to 2, illuminated by a plane wave, is also examined. The distance of the absorber from the cube is 0.1λ and the near-field surface current distribution, along an E-plane loop, is given in Fig. 6. The HO ND-PML is proven to be very powerful, stable and convergent especially at the back of the cube (point D), where the accurate field computation (with the ABC so closely imposed) would be, otherwise, very difficult.

Finally, the high near-grazing incidence absorption of the ND-PML's is investigated in the following experiment. By properly adjusting the simulation time, we assume reflection from one side of a 2-D domain and neglect it from its other sides. The source (22) is positioned two cells above the boundary and an observation point is selected so that waves impinge on the boundary with highly oblique angles (greater than 84 degrees). The depth of the absorber is 0.2λ. It is evident from Fig. 7 that the ND-PML presents a very promising performance for a wide range of frequencies.

V. Conclusions

A new generalized nondiagonally anisotropic PML for wide-angle absorption in FDTD scattering analysis has been

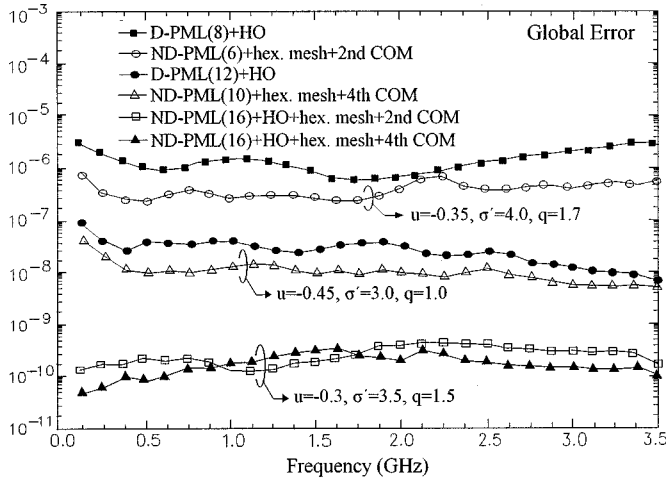

Fig. 7. Frequency spectrum of the global error for various PML's and different discretization (HO, hexagonal) or lattice termination schemes.

presented in this paper. The absorber is constructed through a Maxwellian formulation, while its properties can be selected to provide high attenuation even for the case of the near-grazing incidence, thus being suitable for the treatment of large objects. Higher-order FDTD concepts and non-Cartesian lattices enhance its accuracy and alleviate grid deficiencies. Numerical results prove that the proposed PML offers an essential reduction of domain truncation errors, exhibits sufficient applicability to a variety of irregular boundaries, and requires fairly low computational resources.

REFERENCES

[1] J.-P. Berenger, *J. Comput. Phys.*, vol. 114, pp. 185–200, 1994.
[2] A. Taflove, *Computational Electrodynamics. The Finite-Difference Time-Domain Method*. Boston, MA: Artech House, 1995.
[3] P. Thoma and T. Weiland, *IEEE Trans. Magn.*, vol. 34, pp. 2740–2743, Sept. 1998.
[4] W. C. Chew and W. H. Weedon, *Microwave Opt. Technol. Lett.*, vol. 7, no. 13, pp. 599–604, Sept. 1994.
[5] C. M. Rappaport, *IEEE Microwave Guided Wave Lett.*, vol. 5, no. 3, pp. 90–92, Mar. 1995.
[6] Z. S. Sacks, D. M. Kingsland, R. Lee, and J.-F. Lee, *IEEE Trans. Antennas Propagat*, vol. 43, no. 12, pp. 1460–1463, Dec. 1995.
[7] D. M. Kingsland, J. Kong, J. L. Volakis, and J.-F. Lee, *IEEE Trans. Antennas Propagat.*, vol. 44, no. 7, pp. 975–982, Jul. 1996.
[8] L. Zhao and A. C. Cangellaris, *IEEE Trans. Microwave Theory Tech.*, vol. 44, no. 12, pp. 2555–2563, Dec. 1996.
[9] J. Fang and Z. Wu, *IEEE Microwave Guided Wave Lett.*, vol. 5, no. 12, pp. 451–453, Dec. 1995.
[10] S. D. Gedney, *Electromagn.*, vol. 16, no. 4, pp. 399–415, 1996.
[11] R. W. Ziolkowski, *IEEE Trans. Antennas Propagat.*, vol. 45, no. 3, pp. 1530–1535, Mar. 1997.
[12] Z. Chen, J. Xu, and J.-G. Ma, *IEEE Microwave Guided Wave Lett.*, vol. 9, no. 3, pp. 93–95, Mar. 1999.
[13] N. Harada and M. Hano, *IEEE Microwave Guided Wave Lett.*, vol. 7, no. 7, pp. 335–337, Jul. 1997.
[14] P. G. Petropoulos, L. Zhao, and A. C. Cangellaris, *J. Comput. Phys.*, vol. 139, pp. 184–208, 1998.
[15] T. V. Yioultsis, T. D. Tsiboukis, and E. E. Kriezis, *IEEE Trans. Magn.*, vol. 34, no. 5, pp. 2732–2735, Sept. 1998.
[16] O. M. Ramahi, *J. Comput. Phys.*, vol. 133, pp. 113–128, 1997.